THE JOURNAL OF PHYSICAL CHEMISTRY LETTERS
A JOURNAL OF THE AMERICAN CHEMICAL SOCIETY

pubs.acs.org/JPCL

Perspective

Latent Representation Learning for Structural Characterization of Catalysts

Prahlad K. Routh,[▽] Yang Liu,[▽] Nicholas Marcella,[▽] Boris Kozinsky, and Anatoly I. Frenkel*

Cite This: *J. Phys. Chem. Lett.* 2021, 12, 2086−2094

Read Online

ACCESS | Metrics & More | Article Recommendations | Supporting Information

ABSTRACT: Supervised machine learning-enabled mapping of the X-ray absorption near edge structure (XANES) spectra to local structural descriptors offers new methods for understanding the structure and function of working nanocatalysts. We briefly summarize a status of XANES analysis approaches by supervised machine learning methods. We present an example of an autoencoder-based, unsupervised machine learning approach for latent representation learning of XANES spectra. This new approach produces a lower-dimensional latent representation, which retains a spectrum−structure relationship that can be eventually mapped to physicochemical properties. The latent space of the autoencoder also provides a pathway to interpret the information content "hidden" in the X-ray absorption coefficient. Our approach (that we named latent space analysis of spectra, or LSAS) is demonstrated for the supported Pd nanoparticle catalyst studied during the formation of Pd hydride. By employing the low-dimensional representation of Pd K-edge XANES, the LSAS method was able to isolate the key factors responsible for the observed spectral changes.

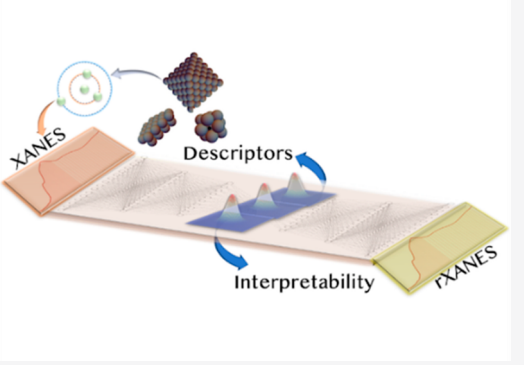

Supported nanoparticles (NPs) have been the focus of in-depth research for developing catalysts that promote sustainability[1] because of their high surface-to-volume ratio and tunable structural, morphological, electronic, and compositional properties.[2−6] Restructuring of catalysts in response to pretreatment and activation and/or during catalysis has also been heavily studied.[7−9] To understand the structure−function relationship in NP catalysts, it is therefore required to probe their atomic and electronic structure in real time, during operating conditions. A vast number of tools exist for carrying out such investigations, ranging from spectroscopy[10−13] to scattering[14,15] and imaging,[16] that are compatible with the *in situ* measurement mode, albeit with their own strengths and weaknesses.[17] For example, techniques sensitive to changes in electronic structure, such as UV−vis absorption, fluorescence spectroscopy, and X-ray photoelectron spectroscopy, can be used to monitor charge transfer associated with metal−metal, metal−adsorbate, and/or metal−support interactions. Techniques sensitive to atomic-level configurational changes, such as Raman spectroscopy, X-ray diffraction, transmission electron microscopy, and scanning transmission electron microscopy, can record the information on molecule structures, phase changes, and changes in particle size and elemental composition, which can be correlated with the catalytic performance.[18−20] Another technique, X-ray absorption fine structure (XAFS) spectroscopy, is an element-specific technique for probing the local structural, electronic, and dynamic properties in NPs, and it is commonly used for *in situ*/*operando* modes.[21−23]

In XAFS, X-ray photons of energy corresponding to that of the core-level electron transition (K, L_1, L_2, L_3, *etc.*) in atomic species of interest are absorbed, causing an increase (known as the absorption edge) of the X-ray absorption coefficient.[24] When the absorption coefficient is measured as a function of the X-ray energy in the region from *ca.* 200 eV below to *ca.* 1000−1500 eV above the absorption edge, the fine structure is obtained in the near-edge and extended regions. The X-ray absorption near edge structure (XANES) is dominated by electronic transitions and multiple scattering processes in the nearest environment to the absorber; thus, it encodes information regarding local electronic and geometric information.[25−27] The extended X-ray absorption fine structure (EXAFS) is due to the interference between the outgoing and incoming photoelectron waves, scattered off neighboring atoms.[28] Because of the short lifetime of the excited state (*ca.* 1 fs) and finite mean free path of the photoelectron, XANES and EXAFS probe the local environment around the absorbing atoms within the first few coordination spheres only, thus enabling the study of the dynamics of local atomic vibrations and structure in a broad range of materials, from crystalline to

Received: December 23, 2020
Accepted: February 16, 2021

https://dx.doi.org/10.1021/acs.jpclett.0c03792
J. Phys. Chem. Lett. 2021, 12, 2086−2094

amorphous to liquids.[9,12,24,29−35] For decades, EXAFS has been the primary source of quantitative information in terms of structural descriptors such as coordination number (N), interatomic distance (R), and mean squared deviation in the interatomic distances (σ^2) (the Debye−Waller factor),[36] enabled by theoretical codes (*e.g.*, FEFF[37] and GNXAS[38]) and readily available fitting software (*e.g.*, IFEFFIT,[39] Demeter,[40] EXCURVE,[41] and GNXAS[38]). XANES, on the other hand, has been relatively less utilized for quantitative structural studies, until recently invented applications of machine learning (ML) methods for the "inversion" of XANES.[42−46]

For example, the use of neural networks (NNs) to invert the XANES (and, as recently demonstrated, EXAFS)[47,48] spectral features was used to successfully obtain coordination numbers and distances from the XANES of monometallic[42,46] and bimetallic[45] nanoparticles and the metal component of oxide clusters.[44] Zheng *et al.* and Torrisi *et al.* used another approach, a random forest ML model, to analyze transition-metal K-edges, to elucidate the local coordination environment of transition-metal oxides in terms of coordination motifs,[49] coordination numbers, distances, and Bader charges.[50] Work has also been done for the analysis of XANES from the oxygen K-edge (O K-edge). Mizoguchi *et al.* combined the decision trees with a neural network to interpret the hidden structural information from the O K-edge XANES of silica polymorphs.[51] Li *et al.* found a neural network model was able to extract the O−Fe coordination number from O K-edge XANES of $Li_3FeO_{3.5}$.[52] Kiyohara *et al.* were able to obtain the radial distribution function from the O K-edge XANES of α-quartz with the assistance of neural networks.[53]

The models summarized above are discriminative by nature and are trained on a labeled data set (constructed from spectra generated theoretically) to identify features which can be further mapped to specific descriptors. While feature engineering is an area where human experts are often needed, in order for the ML methods to fundamentally understand the spectrum−structure relationship, the ML model needs to be able to learn to identify and disentangle the underlying explanatory factors hidden in the data. We note that ensemble methods such as random forests, which have built-in feature importance as an interpretable criterion,[54] and other approaches[55] are being developed to make machine learning models inherently interpretable. Ideally, an interpretable model should have learned structure and parameters which reflect the true causal structure to enable causal interpretations in science.[56] In this regard, unsupervised training or self-supervised training, which are not biased toward specific labels, can provide several additional advantages: better generalization outside training examples, encoding of specific spectral features, and ability to extrapolate between training distributions.[57] Unlike a supervised approach, which is limited by our *a priori* assumptions about the system (*i.e.*, which physical factors or descriptors we believe change as a response to environmental and operating conditions), the unsupervised approach can yield a latent space that contains information about the physically relevant factors without explicitly limiting that space to the known or assumed factors only. Furthermore, as we show in this Perspective, the low-dimensional latent representation learnt by adopting an unsupervised approach can be mapped to important physicochemical properties, such as interatomic distances, coordination numbers, and other structural and electronic descriptors of working catalysts. As a proof of a concept, we use experimental XAFS data obtained in a prototypical catalytic system, namely, supported Pd NPs, undergoing structural and electronic changes under exposure to hydrogen. We performed the unsupervised identification of the important factors which drive the variations in the recorded XAFS spectra during a catalytic reaction. To achieve this objective, we developed a latent space analysis of spectra (LSAS) approach, which aims to develop a low-dimensional representation of input data and characterize the latent space dimensions that are sufficient for recreating the original spectra. We demonstrate the LSAS approach using examples ranging from theoretically generated to the experimentally measured data. In the next section, we provide a brief review of ML methods for physical chemistry applications, and among its many benefits, we highlight their efficacy to extract most important features with relevant signals for classification or descriptor extraction.

The low-dimensional latent representation learned by adopting an unsupervised approach can be mapped to important physicochemical properties, such as interatomic distances, coordination numbers, and other structural and electronic descriptors of working catalysts.

In supervised ML, the goal is to find a function that maps the feature space to a label space, which could be either structural descriptors or categorical variables for identification of different phases or materials. Typical examples for tasks in supervised learning are classification and regression, where the loss function (usually mean squared error or cross entropy) between true labels (or descriptors) and observed estimates is minimized. While the universal approximation theorem of neural networks supports that NNs with one hidden layer and a large enough number of nodes can be approximated to any nonlinear continuous function,[58,59] in practice often powerful variants such as convolutional neural network (CNN) or recurrent neural network (RNN) are used in order to obtain optimal performance.[60] For the ML-assisted XANES and EXAFS data analysis methods, our prior work[44,45,61] has utilized a multilayer perceptron (MLP) to link the data (a spectrum) to structural descriptors (coordination numbers, bond lengths, and/or pair distribution functions) using supervised learning.[44,45]

Unsupervised ML is a class of learning algorithms which do not require labeled data. The goal of these learning algorithms is to recover some underlying structure in the data set. A typical example is data clustering where input data are assigned into groups in such a way that each group has some common properties. Such clusters can sometimes provide interpretable ways of classifying data when subgroups can be linked to those properties. Basic tools of unsupervised learning such as principal component analysis (PCA), independent component analysis (ICA), matrix completion, *etc.* have been used regularly in physical sciences to identify independent species.[60,62] However, predicting physicochemical properties has been difficult using these unsupervised learning methods,

https://dx.doi.org/10.1021/acs.jpclett.0c03792
J. Phys. Chem. Lett. 2021, 12, 2086−2094

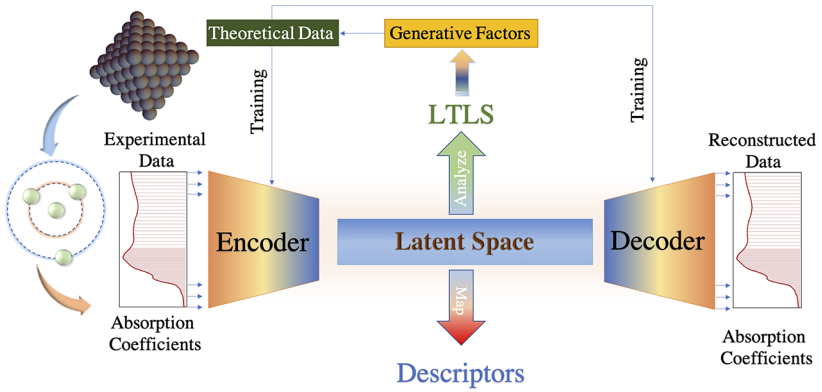

Figure 1. Schematic of the LSAS approach. The autoencoder is trained using theoretical data with known generative factors to learn the low-dimensional latent space in an unsupervised manner. Latent space can be used to (1) analyze the information content and (2) map to physical descriptors.

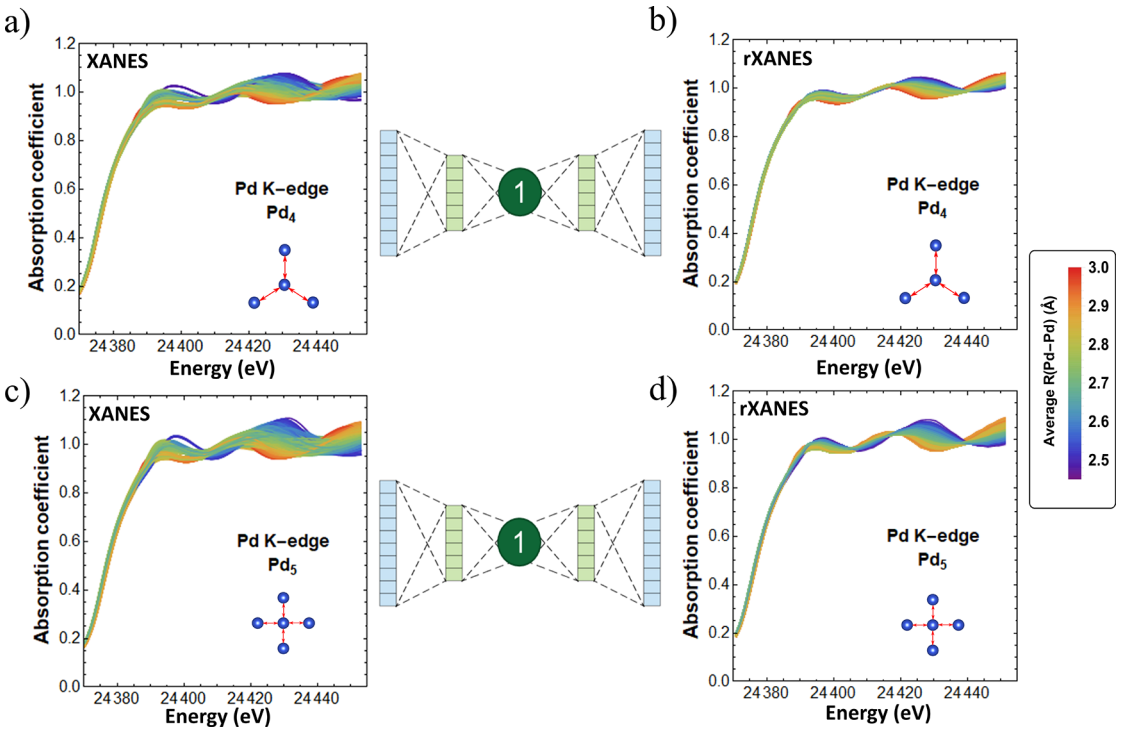

Figure 2. Autoencoder network with one node in bottleneck layer for reconstruction task of reproducing theoretical XANES of Pd atomic clusters: original (a and c) and reconstructed (b and d). The color scale denotes the known interatomic distance used to generate the training data.

and the experimental collection of a large number of data sets is cumbersome for supervised learning.[62] Autoencoders, on the other hand, have been shown to be a versatile NN architecture to create compressed latent representations with low dimensionality. Autoencoders use input data also as the output for training a reconstruction task, while passing the information through a bottleneck layer. Such modern unsupervised and generative models allow for learning latent variables as well as the probability distributions from which new examples can be generated. The goal of generative modeling is to represent, learn, and sample from high-dimensional probability distributions.[63] A variational autoencoder extends the application of an autoencoder using variational inference and a bayesian approach while performing dimensionality reduction from input space into the latent space.[64] Very often different dimensions in the latent space acquire semantic meaning. Such low-dimensional representations have been shown to encode features which are a direct representation of identifiable attributes of input data, *e.g.*, slanted digits and presence/absence of facial hair, in the standard training data set.[65] As a result, arithmetic operations in the latent space can interpolate between physically measurable descriptors. Such an approach of representation learning using deterministic or stochastic autoencoders would be an alternative approach to better established ML methods of XANES analysis by keeping all the features of the nanomaterials that affect the XANES spectrum (and not only selected and arbitrarily chosen descriptors) in the low-dimensional representation where the correlation between the latent features and structural descriptors can be more easily created and interpreted.[66] We hypothesize that low-dimensional latent representations allow the exploration of underlying generative factors, and using this approach, the catalyst's structural and electronic properties can be directly linked to the values encoded in the disentangled latent space

https://dx.doi.org/10.1021/acs.jpclett.0c03792
J. Phys. Chem. Lett. 2021, 12, 2086−2094

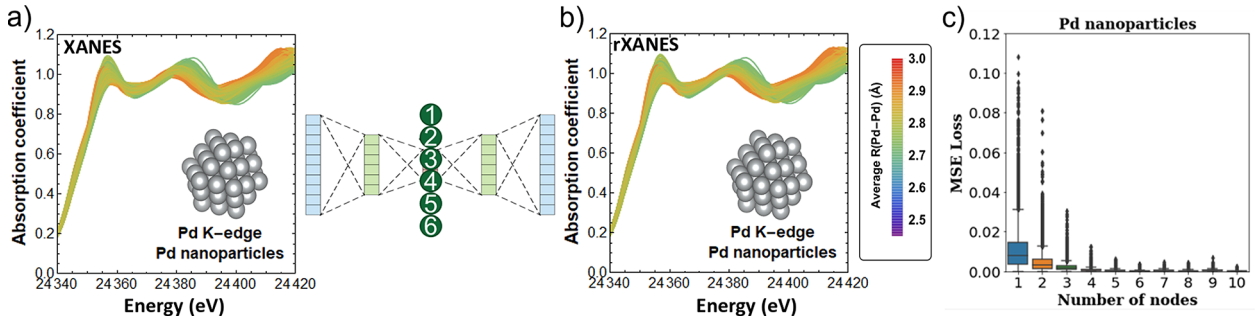

Figure 3. Autoencoder network with six nodes in the bottleneck layer for reconstruction task of reproducing theoretical XANES of Pd nanoparticles: original (a) and reconstructed (b). Color scale denotes the known interatomic distance used to generate the training data. (c) Reconstruction loss (MSE loss) for autoencoder network with increasing number of nodes in bottleneck layer. The box-whisker plot of MSE loss also denotes the median, interquartile range, along with maximum and minimum values. Outliers are plotted as dots. The test data set included 9400 spectra. A semilog plot of MSE loss is shown in Figure S3 of the Supporting Information.

for which the traditional analysis can hardly provide such information. The condensed representation of the nanoparticle information can also expedite the discovery of new materials by correlating the latent features directly with the reaction activity of the materials.[67]

In the next section, we demonstrate an autoencoder-based representation learning approach for characterizing nanocatalysts using their X-ray absorption spectra. A schematic of our overall approach is shown in the Figure 1, which highlights the process of obtaining low-dimensional latent representations of X-ray absorption spectra. This autoencoder is trained using a larger set of theoretical spectra with known generative factors. During the training, the encoder and decoder parameters are learned using a reconstruction task of input data without any labels. This trained network can now be used to generate a latent representation of new theoretical as well as experimental data. As highlighted in the schematic (Figure 1), such a low-dimensional representation can be used for two different tasks: (1) analysis and (2) mapping. In the absence of the *a priori* information about generative factors, this latent representation can be used to conduct correlative analysis on the collection of spectra to uncover underlying factors responsible for the observed changes. However, such study would also require the latent representation to produce unentangled components. We propose applying PCA for this purpose, which would produce a linear transformation of latent space (LTLS). Furthermore, with this knowledge of generative factors, we can train a neural network with latent space as the input layer to map it to the desired descriptors.

We illustrate our approach by using the example of 2.1 ± 0.4 nm Pd nanoparticles supported on Al_2O_3 support (Pd/Al_2O_3) under H_2 and He atmospheres, which was previously analyzed using EXAFS.[68] Pd bulk and nanoparticles readily dissociate H_2, leading to the formation of Pd hydride in fully Pd-coordinated octahedral sites.[27,68,69] The Pd hydride formation is accompanied by up to a 3.9% increase in the lattice parameter of Pd (for the maximum amount of Pd hydride formation in the β phase of bulk Pd: $PdH_{0.72}$)[70] and for lesser degrees in nanoparticles, depending on the NP size, shape, temperature, and H_2 pressure.[27,68,71,72] The Pd/Al_2O_3 NPs had narrow size distribution and were collected at 20, 110, and 210 °C under 1 atm of H_2 and 20, 110, and 210 °C under 1 atm of He to determine the amount of Pd hydride as a function of temperature. This data is a perfect test case for the new method because we know, independently, their structural changes from prior EXAFS analysis.

We first turn our attention to a model system of atomic clusters of Pd composed of 2, 3, 4, and 5 atoms (Figures S1 and 2a–d) in which interatomic distances were varied for generating (using FEFF9) the series of XANES spectra averaged over all absorbers in the cluster. A similar theoretical XANES data set was developed for larger Pd nanoparticles, which were composed of Pd atoms ranging from 6 to 165, along with multiple variations (shape, size, interatomic distance, and hydrogen fraction) in their structure (see the Supporting Information for more details).

Low-Dimensional Representation Learning of Theoretical Spectra. In order to reduce the dimensionality and learn latent representations, we train the autoencoder with a reconstruction task. The number of nodes in the bottleneck layer defines the dimensionality of latent representation. Recently, it has been asserted that the number of independent nodes in latent representation is equal to the degree of freedom of the training data.[73] However, in the machine learning literature, the question of the optimal number of nodes required to reconstruct the original spectra is not clearly addressed, and the most common latent space dimension is chosen on an *ad hoc* basis.

We systematically probed the reconstruction loss, measured using mean squared error (MSE) loss between original spectra and reconstructed spectra, with a varying number of nodes in the latent space. As intuitively expected, we observed a decrease and subsequent stabilization in the reconstruction loss with increase in latent space dimensions (number of nodes in the bottleneck). We observe that for the simulated XANES of simple atomic clusters, encoder and decoder can be trained to reconstruct the spectra with the bottleneck layer composed of as low as 1 node (see Figures 2 and S2 for reconstructed spectra). However, for the case of simulated XANES spectra of Pd nanoparticles (Figure 3a,b) the number of nodes needed in the bottleneck is at least 6 nodes (*vide infra*) as inferred from a minimum in the MSE loss shown in Figures 3c and S3. A crossover between the two trends in reconstruction loss provides not only the approximate dimension of latent space needed for reconstruction but also the approximate number of "hidden" physicochemical factors which can explain the variation in the data, providing us with an estimate of information content.

Exploration of Latent Space in Model Pd Atomic Cluster. In order to determine whether the latent representation obtained by unsupervised training encodes physical factors (in general, these are not known *a priori*), we have to first find a way to

https://dx.doi.org/10.1021/acs.jpclett.0c03792
J. Phys. Chem. Lett. 2021, 12, 2086–2094

interpret the latent space after unsupervised training. One way to do this is to study the correlation between each latent space dimension and the real space descriptors (bond lengths, coordination numbers, *etc.*) of the theoretically generated XANES spectra used in unsupervised training. In doing so, we observe a high degree of correlations (Figure 4) between the

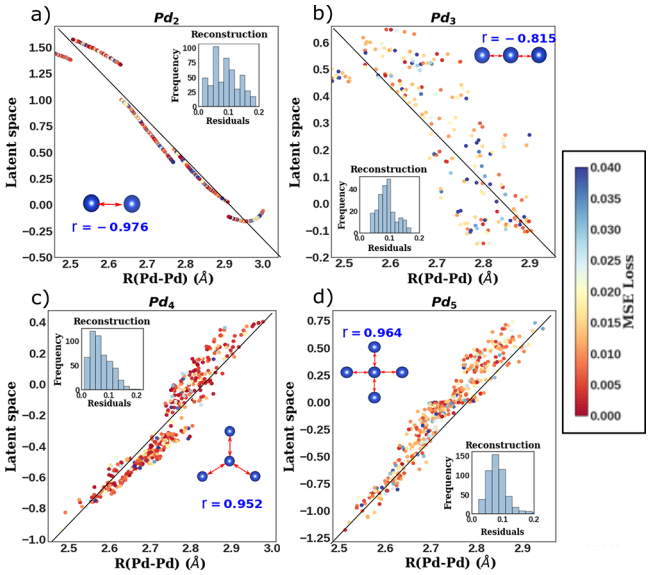

Figure 4. True R(Pd−Pd) Å versus the latent variables in the bottleneck layer. The histogram of residuals between true and reconstructed spectra exhibits the performance of our autoencoders. The values for the Pearson correlation coefficient are shown near each atomic cluster. The color of the dots denotes the data points with varying quality of reconstruction distributed randomly in the whole range of R(Pd−Pd) and indicating that the reconstruction error has no correlation with the R(Pd−Pd).

latent node encoding and average interatomic distance, where indeed, interatomic distance is the generative factor behind the distributions of data for each Pd atomic cluster. We see the trend continued in Figure 4 for all four model Pd atomic clusters. This provides us with evidence that variation in generative factors can be thus encoded in the latent space.

Exploration of Latent Space in Theoretical XANES of Pd Nanoparticles. For the case of Pd nanoparticles, multiple generative factors were used in combination to obtain a large collection of training data set (see the Supporting Information for more details on training data) to approximate a more realistic situation. Among the physical factors, coordination number (N) and interatomic distance (R) are seen as the most important generative factors encoded in the latent space, based on their relatively localized correlations. Figure 5 visualizes this correlation. Because we aimed to demonstrate our method with Pd NPs in a H_2 environment, we also include variations in hydrogen fraction (H), which is defined as the ratio of Pd octahedral sites which are occupied by hydrogen atoms for a given model. The correlation between H and any given latent space dimension was weak compared to that of N and R, and therefore, changes in H are relatively more distributed over the latent space dimensions.

In general, for a latent space with a dimension greater than 1, we see that the information associated with the physical factors is found to be distributed over multiple nodes and may also be considered entangled with other information, as seen in Figure

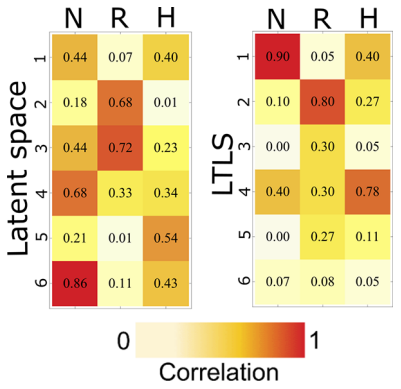

Figure 5. Correlation between the latent space before and after PCA analysis (LTLS) with the descriptors: N(Pd−Pd), R(Pd−Pd), and H, the hydrogen fraction. The values for the Pearson correlation coefficient are shown in each box.

5. While additional conditions on the encoded information in the bottleneck layer can be imposed during autoencoder training (such as VAE with independent Gaussian distribution)[64] by adding constraints on the loss function to produce a disentangled latent space, we show that a linear transformation of latent space, such as using PCA, can partially help disentangle the information content. PCA of the latent representations resulted in linear transformation of latent space and provided orthonormal axes which are found to be independently correlated with physical descriptors, as shown in Figure 5 for our theoretical data set. Latent space analysis, when applied on a collection of XANES spectra, provides more clear interpretation of the factors contributing to the changes observed in a set of XANES spectra.

While the transformed latent space is found to be correlated with the physical descriptors, there is still no way to use PCA to extract the values of the descriptors for individual spectrum, and the correlation can be obtained only if the descriptors are known or assumed *a priori*. Instead of using LSAS for only qualitative analysis, we can use a nonlinear mapping approach (using a neural network) to map the low-dimensional latent representation to the physical descriptors. Figure 6 shows the prediction of coordination number, interatomic distance, and fraction of occupied octahedral sites by hydrogen atoms.

Finally, because we are confident that unsupervised training results in a latent space that encodes generative factors, we use the above method to train an autoencoder which produces a low-dimensional representation for experimentally acquired data for analysis and prediction of structural and physicochemical properties.

Analyzing Experimentally Obtained XANES Data in Pd Nanoparticles. In order to obtain a low-dimensional representation of experimentally obtained XANES, we utilized the same approach of reconstruction as a task on the training data using an autoencoder. The encoder and decoder parameters pretrained with a theoretical XANES data set perform reasonably well on the reconstruction task of experimentally obtained XANES despite the slight discrepancy in the theoretical and experimental spectra. Reconstruction performance can be improved further by using convolutional layers in the encoder and decoder and using experimental data during the model selection step as described in our previous work.[42]

To analyze the information content, we trained autoencoders with varied dimensions of latent space during the reconstruction task and observed a minimum reconstruction

https://dx.doi.org/10.1021/acs.jpclett.0c03792
J. Phys. Chem. Lett. 2021, 12, 2086−2094

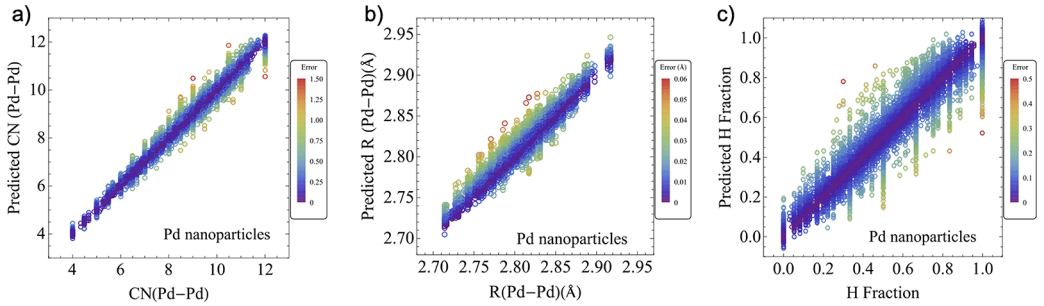

Figure 6. Predicted vs ground truth values of physical factors: (a) coordination number (N), (b) interatomic distance (R), and (c) fraction of occupied octahedral sites by hydrogen atom (H) in Pd nanoparticles. Color scale denotes relative error between the ground truth and the predicted values. The details of the theoretical XANES for Pd nanoparticles are described in section S2 of the Supporting Information.

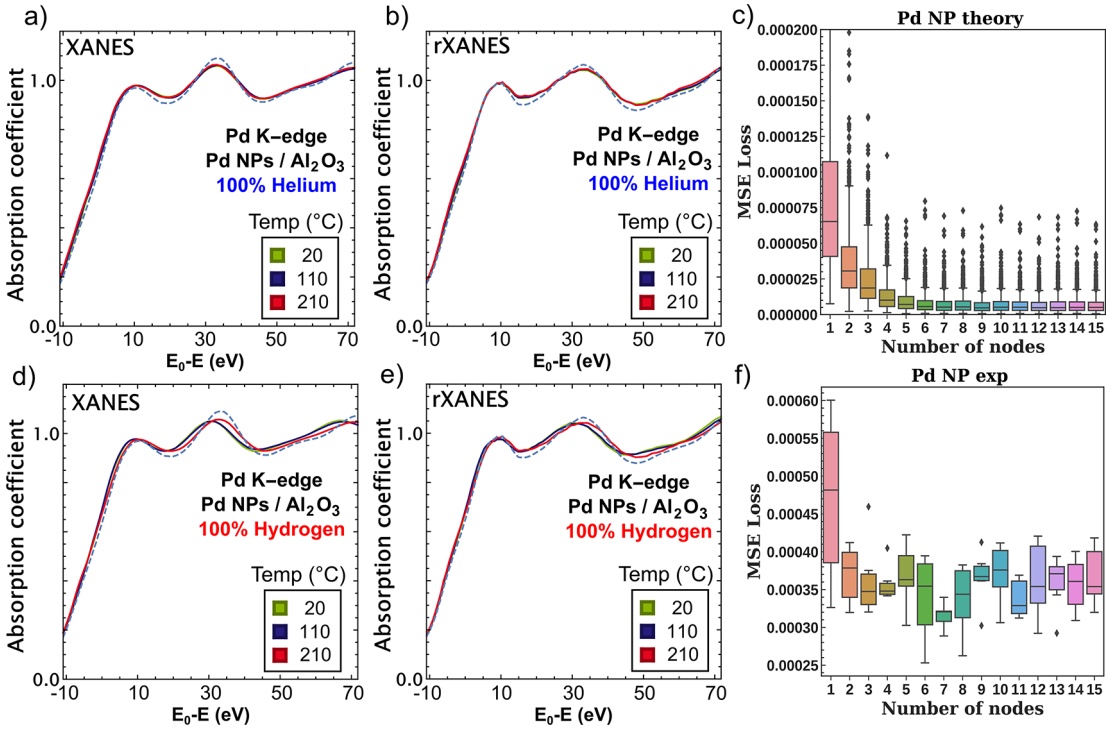

Figure 7. Experimentally obtained XANES (a and d) of Pd nanoparticles supported on Al_2O_3 and its reconstruction (b and e) using autoencoder at various temperature and atmospheric conditions. (c and f) Change in reconstruction loss with varying number of nodes in latent space for theoretical and experimental XANES, respectively. Pd foil spectrum, collected at the same time as the experiment, is plotted in (a, b, d, e) with a gray dashed curve.

loss with around 7 nodes for the experimental data set (Figure 7). The autoencoder architecture is described in Figure S4. This low-dimensional representation encompasses all of the information needed to reconstruct the experimental XANES using the decoder, as depicted by pairwise comparison in Figures 7a,b and 7d,e, and exhibits very good agreement across various temperatures in both hydrogen and helium atmospheres. The application of PCA (Figure 8a) on the complete set of experimental data elucidates that there are at least two components required to explain the variance observed in the latent space representation.

Given the orthonormal transformation provided by PCA, we conclude that there are at least two independent underlying factors which give rise to the variation in the experimental XANES. The correlation of the first principal component with interatomic distance (Figure 8a) confirms our hypothesis that latent space captures the primary underlying generative factor. The second principal component of latent space shows weak correlation with the fraction of octahedral sites occupied by hydrogen. Because the absorbed fraction (H/Pd) of hydrogen in bulk and nanoscale Pd hydride is known to have a one-to-one correspondence with the interatomic Pd–Pd distance,[74] we interpret the nonzero second principal component to be not directly related to the hydrogen absorption effect. It can reflect, for example, the effect of increased bond length disorder due to the increased bond vibration amplitude at elevated temperature and requires further investigation.

The overall utility of our approach lies in the ease of extraction of physical parameters which have been verified by analyzing the latent space. With this analysis, we have observed a strong correlation between latent space and a known causal factor which supports the body of conclusive evidence that interatomic distance is indeed a primary factor for the observed variation in the analyzed set of experimental XANES. Furthermore, we mapped this low-dimensional latent representation to physical factors using a multilayered perceptron

https://dx.doi.org/10.1021/acs.jpclett.0c03792
J. Phys. Chem. Lett. 2021, 12, 2086–2094

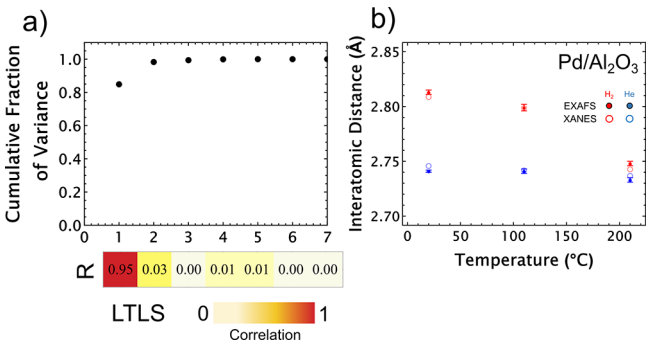

Figure 8. (a) Cumulative fraction of variance of experimentally obtained XANES of Pd nanoparticles supported on Al_2O_3 after linear transformation of latent space (LTLS). Correlation map along with Pearson correlation coefficient between LTLS and interatomic distance shown below *x*-axis. (b) Comparison of interatomic distances mapped with latent space with corresponding data obtained via EXAFS analysis.

The overall utility of our approach lies in the ease of extraction of physical parameters which have been verified by analyzing the latent space.

and compare it with descriptors obtained by traditional EXAFS analysis. Figure 8b shows excellent agreement between predicted and ground truth (analyzed by EXAFS) interatomic distances. The parameters of the MLP used for this mapping are described in Figure S5.

Our LSAS approach provides a transparent way to analyze and interpret the mapping of experimentally obtained XANES to the interatomic Pd−Pd distances and hence offers a complementary and perhaps powerful alternative to EXAFS analysis. This method can be extended to inversion of XANES to various other descriptors such as coordination number and particle sizes which may be difficult to obtain with EXAFS analysis. Moreover, with the advantage of reduced dimensionality and inversion capability, this method can be used to observe dynamic changes in the catalytic process at different temperatures which could be advantageous for *in situ* methods.

As part of the concluding remarks, we note that representational learning has shown to be a significant milestone in the machine learning community, especially for imaging data. We attempted to translate these recent developments in ML applications for the problems relevant for physical chemistry, such as structural and mechanistic studies of nanocatalysts. We have shown that exploring low-dimensional representation of XANES spectra in nanocatalysts can be a valuable tool for analyzing information content in the XANES signal. We have also shown the ability to extract the descriptors from the XANES spectrum using an autoencoder approach coupled with the neural network analysis of latent space. In the examples shown in this Perspective, we have focused only on the deterministic layers of the encoder and decoder blocks. However, the method can be improved drastically with the careful use of stochastic autoencoders as well. This low-dimensional latent space can be further dimensionally reduced to visualize and observe the clustering of input data (that signal the same physicochemical properties) for further analysis, based on the known or assumed structures or other interpretable generative factors.

■ ASSOCIATED CONTENT

Supporting Information

The Supporting Information is available free of charge at https://pubs.acs.org/doi/10.1021/acs.jpclett.0c03792.

Details of XANES simulation by FEFF9 for Pd atomic clusters and Pd nanoparticles; autoencoder architecture used for the latent representation learning and prediction of the structural descriptors of the Pd nanoparticles (PDF)

■ AUTHOR INFORMATION

Corresponding Author

Anatoly I. Frenkel − *Department of Materials Science and Chemical Engineering, Stony Brook University, Stony Brook, New York 11794, United States; Division of Chemistry, Brookhaven National Laboratory, Upton, New York 11973, United States;* orcid.org/0000-0002-5451-1207; Email: anatoly.frenkel@stonybrook.edu

Authors

Prahlad K. Routh − *Department of Materials Science and Chemical Engineering, Stony Brook University, Stony Brook, New York 11794, United States*

Yang Liu − *Department of Materials Science and Chemical Engineering, Stony Brook University, Stony Brook, New York 11794, United States*

Nicholas Marcella − *Department of Materials Science and Chemical Engineering, Stony Brook University, Stony Brook, New York 11794, United States;* orcid.org/0000-0002-2224-532X

Boris Kozinsky − *John A. Paulson School of Engineering and Applied Sciences, Harvard University, Cambridge, Massachusetts 02138, United States; Bosch Research, Cambridge, Massachusetts 02139, United States;* orcid.org/0000-0002-0638-539X

Complete contact information is available at: https://pubs.acs.org/10.1021/acs.jpclett.0c03792

Author Contributions

[▽]P.K.R., Y.L., and N.M. contributed equally to this work.

Notes

The authors declare no competing financial interest.

■ ACKNOWLEDGMENTS

The work was supported as part of the Integrated Mesoscale Architectures for Sustainable Catalysis (IMASC), an Energy Frontier Research Center funded by the U.S. Department of Energy, Office of Science, Basic Energy Sciences under Award No. DE-SC9912573. This research used resources of the Center for Functional Nanomaterials, which is a U.S. DOE Office of Science Facility, and the Scientific Data and Computing Center, a component of the Computational Science Initiative, at Brookhaven National Laboratory under Contract No. DE-SC0012704. X-ray absorption spectra for Pd nanoparticles used in this work (also published in ref 68) were obtained at beamline X18B of National Synchrotron Light Source of Brookhaven National Laboratory.

REFERENCES

(1) Friend, C. M.; Xu, B. Heterogeneous Catalysis: A Central Science for a Sustainable Future. *Acc. Chem. Res.* **2017**, *50*, 517−521.
(2) Haruta, M. When Gold Is Not Noble: Catalysis by Nanoparticles. *Chem. Rec.* **2003**, *3*, 75−87.
(3) Guliamov, O.; Frenkel, A. I.; Menard, L. D.; Nuzzo, R. G.; Kronik, L. Tangential Ligand-Induced Strain in Icosahedral Au13. *J. Am. Chem. Soc.* **2007**, *129*, 10978−10979.
(4) Mostafa, S.; Behafarid, F.; Croy, J. R.; Ono, L. K.; Li, L.; Yang, J. C.; Frenkel, A. I.; Cuenya, B. R. Shape-Dependent Catalytic Properties of Pt Nanoparticles. *J. Am. Chem. Soc.* **2010**, *132*, 15714−15719.
(5) Zhang, L.; Henkelman, G. Computational Design of Alloy-Core@Shell Metal Nanoparticle Catalysts. *ACS Catal.* **2015**, *5*, 655−660.
(6) Li, Y.; Zakharov, D.; Zhao, S.; Tappero, R.; Jung, U.; Elsen, A.; Baumann, P.; Nuzzo, R. G.; Stach, E. A.; Frenkel, A. I. Complex Structural Dynamics of Nanocatalysts Revealed in Operando Conditions by Correlated Imaging and Spectroscopy Probes. *Nat. Commun.* **2015**, *6*, 7583.
(7) Choi, Y.-W.; Mistry, H.; Roldan Cuenya, B. New Insights into Working Nanostructured Electrocatalysts through Operando Spectroscopy and Microscopy. *Curr. Opin. Electrochem.* **2017**, *1*, 95−103.
(8) Luneau, M.; Guan, E.; Chen, W.; Foucher, A. C.; Marcella, N.; Shirman, T.; Verbart, D. M. A.; Aizenberg, J.; Aizenberg, M.; Stach, E. A.; et al. Enhancing Catalytic Performance of Dilute Metal Alloy Nanomaterials. *Commun. Chem.* **2020**, *3*, 46.
(9) Nashner, M. S.; Frenkel, A. I.; Adler, D. L.; Shapley, J. R.; Nuzzo, R. G. Structural Characterization of Carbon-Supported Platinum-Ruthenium Nanoparticles from the Molecular Cluster Precursor PtRu5C(CO)(16. *J. Am. Chem. Soc.* **1997**, *119*, 7760−7771.
(10) Frenkel, A. I.; Rodriguez, J. A.; Chen, J. G. Synchrotron Techniques for In Situ Catalytic Studies: Capabilities, Challenges, and Opportunities. *ACS Catal.* **2012**, *2*, 2269−2280.
(11) Surnev, S.; Ramsey, M. G.; Netzer, F. P. Synchrotron Radiation Applied to the Study of Heterogeneous Model Catalyst Surfaces. *J. Phys.: Condens. Matter* **2001**, *13*, 11305−11332.
(12) Singh, J.; Lamberti, C.; van Bokhoven, J. A. Advanced X-Ray Absorption and Emission Spectroscopy: In Situ Catalytic Studies. *Chem. Soc. Rev.* **2010**, *39*, 4754−4766.
(13) Stavitski, E.; Weckhuysen, B. M. Infrared and Raman Imaging of Heterogeneous Catalysts. *Chem. Soc. Rev.* **2010**, *39*, 4615−4625.
(14) Herklotz, M.; Scheiba, F.; Hinterstein, M.; Nikolowski, K.; Knapp, M.; Dippel, A.-C.; Giebeler, L.; Eckert, J.; Ehrenberg, H. Advances in in Situ Powder Diffraction of Battery Materials: A Case Study of the New Beamline P02.1 at DESY, Hamburg. *J. Appl. Crystallogr.* **2013**, *46*, 1117−1127.
(15) Stavitski, E.; Beale, A. M.; Weckhuysen, B. M. Catalyst Characterization—Heterogeneous. In *Encyclopedia of Catalysis*; Horváth, I., Ed.; Wiley, 2010.
(16) Beale, A. M.; Jacques, S. D. M.; Weckhuysen, B. M. Chemical Imaging of Catalytic Solids with Synchrotron Radiation. *Chem. Soc. Rev.* **2010**, *39*, 4656−4672.
(17) Weckhuysen, B. M. *In-Situ Spectroscopy of Catalysts*; American Scientific Publishers, 2004.
(18) Rao, R.; Pierce, N.; Liptak, D.; Hooper, D.; Sargent, G.; Semiatin, S. L.; Curtarolo, S.; Harutyunyan, A. R.; Maruyama, B. Revealing the Impact of Catalyst Phase Transition on Carbon Nanotube Growth by in Situ Raman Spectroscopy. *ACS Nano* **2013**, *7*, 1100−1107.
(19) Couves, J. W.; Thomas, J. M.; Waller, D.; Jones, R. H.; Dent, A. J.; Derbyshire, G. E.; Greaves, G. N. Tracing the Conversion of Aurichalcite to a Copper Catalyst by Combined X-Ray Absorption and Diffraction. *Nature* **1991**, *354*, 465−468.
(20) Tsoukalou, A.; Abdala, P. M.; Stoian, D.; Huang, X.; Willinger, M. G.; Fedorov, A.; Müller, C. R. Structural Evolution and Dynamics of an In2O3 Catalyst for CO2 Hydrogenation to Methanol: An Operando XAS-XRD and in Situ TEM Study. *J. Am. Chem. Soc.* **2019**, *141*, 13497−13505.
(21) Koningsberger, D. C.; Prins, R. *X-Ray Absorption: Principles, Applications, Techniques of EXAFS, SEXAFS, and XANES*; Wiley,1988.
(22) Stern, E. A.; Zhang, K. Local Premelting about Impurities. *Phys. Rev. Lett.* **1988**, *60*, 1872−1875.
(23) Stern, E. A.; Livņs, P.; Zhang, Z. Thermal Vibration and Melting from a Local Perspective. *Phys. Rev. B: Condens. Matter Mater. Phys.* **1991**, *43*, 8850−8860.
(24) Bunker, G. *Introduction to XAFS: A Practical Guide to X-Ray Absorption Fine Structure Spectroscopy*; Cambridge University Press, 2010.
(25) Rehr, J. J.; Albers, R. C.; Zabinsky, S. I. High-Order Multiple-Scattering Calculations of x-Ray-Absorption Fine Structure. *Phys. Rev. Lett.* **1992**, *69*, 3397−3400.
(26) Ankudinov, A. L.; Rehr, J. J.; Low, J. J.; Bare, S. R. Sensitivity of Pt X-Ray Absorption near Edge Structure to the Morphology of Small Pt Clusters. *J. Chem. Phys.* **2002**, *116*, 1911−1919.
(27) Bugaev, A. L.; Guda, A. A.; Lazzarini, A.; Lomachenko, K. A.; Groppo, E.; Pellegrini, R.; Piovano, A.; Emerich, H.; Soldatov, A. V.; Bugaev, L. A.; et al. In Situ Formation of Hydrides and Carbides in Palladium Catalyst: When XANES Is Better than EXAFS and XRD. *Catal. Today* **2017**, *283*, 119−126.
(28) Zabinsky, S. I.; Rehr, J. J.; Ankudinov, A.; Albers, R. C.; Eller, M. J. Multiple-Scattering Calculations of X-Ray-Absorption Spectra. *Phys. Rev. B: Condens. Matter Mater. Phys.* **1995**, *52*, 2995−3009.
(29) Rehr, J. J.; Albers, R. C. Theoretical Approaches to X-Ray Absorption Fine Structure. *Rev. Mod. Phys.* **2000**, *72*, 621−654.
(30) Penner-Hahn, J. E. X-Ray Absorption Spectroscopy in Coordination Chemistry. *Coord. Chem. Rev.* **1999**, *190−192*, 1101−1123.
(31) Russell, A. E.; Rose, A. X-Ray Absorption Spectroscopy of Low Temperature Fuel Cell Catalysts. *Chem. Rev.* **2004**, *104*, 4613−4636.
(32) Wende, H. Recent Advances in X-Ray Absorption Spectroscopy. *Rep. Prog. Phys.* **2004**, *67*, 2105−2181.
(33) Timoshenko, J.; Roldan Cuenya, B. In Situ/Operando Electrocatalyst Characterization by X-Ray Absorption Spectroscopy. *Chem. Rev.* **2021**, *121*, 882−961.
(34) Filipponi, A. EXAFS for Liquids. *J. Phys.: Condens. Matter* **2001**, *13*, R23−R60.
(35) Hardacre, C. Application of EXAFS to Molten Salts and Ionic Liquid Technology. *Annu. Rev. Mater. Res.* **2005**, *35*, 29−49.
(36) Sayers, D. E.; Stern, E. A.; Lytle, F. W. New Technique for Investigating Noncrystalline Structures: Fourier Analysis of the Extended X-Ray—Absorption Fine Structure. *Phys. Rev. Lett.* **1971**, *27*, 1204−1207.
(37) Rehr, J. J.; Kas, J. J.; Vila, F. D.; Prange, M. P.; Jorissen, K. Parameter-Free Calculations of X-Ray Spectra with FEFF9. *Phys. Chem. Chem. Phys.* **2010**, *12*, 5503−5513.
(38) Hatada, K.; Iesari, F.; Properzi, L.; Minicucci, M.; di Cicco, A. New Graphical User Interface for EXAFS Analysis with the GNXAS Suite of Programs. *J. Phys.: Conf. Ser.* **2016**, *712*, 012002.
(39) Newville, M. IFEFFIT: Interactive XAFS Analysis and FEFF Fitting. *J. Synchrotron Radiat.* **2001**, *8*, 322−324.
(40) Ravel, B.; Newville, M. ATHENA, ARTEMIS, HEPHAESTUS: Data Analysis for X-Ray Absorption Spectroscopy Using IFEFFIT. *J. Synchrotron Radiat.* **2005**, *12*, 537−541.
(41) Tomic, S.; Searle, B. G.; Wander, A.; Harrison, N. M.; Dent, A.; Mosselmans, J. F. W.; Inglesfield, J. E. *The DL EXCURV Package*; STFC Daresbury Laboratory, 2004.
(42) Timoshenko, J.; Lu, D.; Lin, Y.; Frenkel, A. I. Supervised Machine-Learning-Based Determination of Three-Dimensional Structure of Metallic Nanoparticles. *J. Phys. Chem. Lett.* **2017**, *8*, 5091−5098.
(43) Timoshenko, J.; Frenkel, A. I. "Inverting" X-Ray Absorption Spectra of Catalysts by Machine Learning in Search for Activity Descriptors. *ACS Catal.* **2019**, *9*, 10192−10211.
(44) Liu, Y.; Marcella, N.; Timoshenko, J.; Halder, A.; Yang, B.; Kolipaka, L.; Pellin, M. J.; Seifert, S.; Vajda, S.; Liu, P.; et al. Mapping XANES Spectra on Structural Descriptors of Copper Oxide Clusters

https://dx.doi.org/10.1021/acs.jpclett.0c03792
J. Phys. Chem. Lett. 2021, 12, 2086−2094

Using Supervised Machine Learning. *J. Chem. Phys.* **2019**, *151*, 164201.
(45) Marcella, N.; Liu, Y.; Timoshenko, J.; Guan, E.; Luneau, M.; Shirman, T.; Plonka, A. M.; van der Hoeven, J. E. S.; Aizenberg, J.; Friend, C. M.; et al. Neural Network Assisted Analysis of Bimetallic Nanocatalysts Using X-Ray Absorption near Edge Structure Spectroscopy. *Phys. Chem. Chem. Phys.* **2020**, *22*, 18902−18910.
(46) Timoshenko, J.; Halder, A.; Yang, B.; Seifert, S.; Pellin, M. J.; Vajda, S.; Frenkel, A. I. Subnanometer Substructures in Nanoassemblies Formed from Clusters under a Reactive Atmosphere Revealed Using Machine Learning. *J. Phys. Chem. C* **2018**, *122*, 21686−21693.
(47) Timoshenko, J.; Anspoks, A.; Cintins, A.; Kuzmin, A.; Purans, J.; Frenkel, A. I. Neural Network Approach for Characterizing Structural Transformations by X-Ray Absorption Fine Structure Spectroscopy. *Phys. Rev. Lett.* **2018**, *120*, 225502.
(48) Timoshenko, J.; Wrasman, C. J.; Luneau, M.; Shirman, T.; Cargnello, M.; Bare, S. R.; Aizenberg, J.; Friend, C. M.; Frenkel, A. I. Probing Atomic Distributions in Mono- and Bimetallic Nanoparticles by Supervised Machine Learning. *Nano Lett.* **2019**, *19*, 520−529.
(49) Zheng, C.; Chen, C.; Chen, Y.; Ong, S. P. Random Forest Models for Accurate Identification of Coordination Environments from X-Ray Absorption Near-Edge Structure. *Patterns* **2020**, *1*, 100013.
(50) Torrisi, S. B.; Carbone, M. R.; Rohr, B. A.; Montoya, J. H.; Ha, Y.; Yano, J.; Suram, S. K.; Hung, L. Random Forest Machine Learning Models for Interpretable X-Ray Absorption near-Edge Structure Spectrum-Property Relationships. *npj Comput. Mater.* **2020**, *6*, 109.
(51) Mizoguchi, T.; Kiyohara, S. Machine Learning Approaches for ELNES/XANES. *Microscopy* **2020**, *69*, 92−109.
(52) Li, L.; Lu, M.; Chan, M. K. Y. A Deep Learning Model for Atomic Structures Prediction Using X-Ray Absorption Spectroscopic Data. *arXiv* [physics.comp-ph], **2019**, 1905.03928.
(53) Kiyohara, S.; Mizoguchi, T. Radial Distribution Function from X-Ray Absorption near Edge Structure with an Artificial Neural Network. *J. Phys. Soc. Jpn.* **2020**, *89*, 103001.
(54) Breiman, L. Random Forests. *Machine Learning* **2001**, *45*, 5−32.
(55) Chen, Z.; Bei, Y.; Rudin, C. Concept Whitening for Interpretable Image Recognition. *Nat. Mach. Intell.* **2020**, *2*, 772−782.
(56) Molnar, C.; Casalicchio, G.; Bischl, B. Interpretable Machine Learning—A Brief History, State-of-the-Art and Challenges. *arXiv*, **2020**, 2010.09337.
(57) Latif, S.; Rana, R.; Khalifa, S.; Jurdak, R.; Qadir, J. Deep Representation Learning in Speech Processing: Challenges, Recent Advances, and Future Trends. *arXiv*, **2020**, 2001.00378.
(58) Hornik, K.; Stinchcombe, M.; White, H. Multilayer. Feedforward Networks are Universal Approximators. *Neural Networks* **1989**, *2*, 359−366.
(59) Cybenko, G. Approximation by Superpositions of a Sigmoidal Function. *Math. Control. Signals, Syst.* **1989**, *2*, 303−314.
(60) Carleo, G.; Cirac, I.; Cranmer, K.; Daudet, L.; Schuld, M.; Tishby, N.; Vogt-Maranto, L.; Zdeborová, L. Machine Learning and the Physical Sciences. *Rev. Mod. Phys.* **2019**, *91*, No. 045002.
(61) Dias, E. T.; Gill, S. K.; Liu, Y.; Halstenberg, P.; Dai, S.; Huang, J.; Mausz, J.; Gakhar, R.; Phillips, W. C.; Mahurin, S.; et al. Radiation-Assisted Formation of Metal Nanoparticles in Molten Salts. *J. Phys. Chem. Lett.* **2021**, *12*, 157−164.
(62) Jirasek, F.; Alves, R. A. S.; Damay, J.; Vandermeulen, R. A.; Bamler, R.; Bortz, M.; Mandt, S.; Kloft, M.; Hasse, H. Machine Learning in Thermodynamics: Prediction of Activity Coefficients by Matrix Completion. *J. Phys. Chem. Lett.* **2020**, *11*, 981−985.
(63) Foster, D. *Generative deep learning: teaching machines to paint, write, compose, and play*; O'Reilly Media, 2019.
(64) Kingma, D. P.; Welling, M. Auto-Encoding Variational Bayes. *2nd Int. Conf. Learn. Represent. ICLR 2014 - Conf. Track Proc.* 2014; pp 1−14.
(65) Higgins, I.; Matthey, L.; Pal, A.; Burgess, C.; Glorot, X.; Botvinick, M.; Mohamed, S.; Lerchner, A. B-VAE: Learning Basic Visual Concepts with a Constrained Variational Framework. *5th Int. Conf. Learn. Represent. ICLR 2017 - Conf. Track Proc.* 2017; pp 1−22.
(66) Wetzel, S. J. Unsupervised Learning of Phase Transitions: From Principal Component Analysis to Variational Autoencoders. *Phys. Rev. E: Stat. Phys., Plasmas, Fluids, Relat. Interdiscip. Top.* **2017**, *96*, 022140.
(67) Ge, L.; Yuan, H.; Min, Y.; Li, L.; Chen, S.; Xu, L.; Goddard, W. A. Predicted Optimal Bifunctional Electrocatalysts for the Hydrogen Evolution Reaction and the Oxygen Evolution Reaction Using Chalcogenide Heterostructures Based on Machine Learning Analysis of in Silico Quantum Mechanics Based High Throughput Screening. *J. Phys. Chem. Lett.* **2020**, *11*, 869−876.
(68) Wang, J.; Wang, Q.; Jiang, X.; Liu, Z.; Yang, W.; Frenkel, A. I. Determination of Nanoparticle Size by Measuring the Metal−Metal Bond Length: The Case of Palladium Hydride. *J. Phys. Chem. C* **2015**, *119*, 854−861.
(69) Guan, E.; Foucher, A. C.; Marcella, N.; Shirman, T.; Luneau, M.; Head, A. R.; Verbart, D. M. A.; Aizenberg, J.; Friend, C. M.; Stacchiola, D.; et al. New Role of Pd Hydride as a Sensor of Surface Pd Distributions in Pd−Au Catalysts. *ChemCatChem* **2020**, *12*, 717−721.
(70) Davis, R. J.; Landry, S. M.; Horsley, J. A.; Boudart, M. X-Ray-Absorption Study of the Interaction of Hydrogen with Clusters of Supported Palladium. *Phys. Rev. B: Condens. Matter Mater. Phys.* **1989**, *39*, 10580−10583.
(71) Tew, M. W.; Miller, J. T.; van Bokhoven, J. A. Particle Size Effect of Hydride Formation and Surface Hydrogen Adsorption of Nanosized Palladium Catalysts: L-3 Edge vs K Edge X-Ray Absorption Spectroscopy. *J. Phys. Chem. C* **2009**, *113*, 15140−15147.
(72) Suleiman, M.; Jisrawi, N. M.; Dankert, O.; Reetz, M. T.; Bähtz, C.; Kirchheim, R.; Pundt, A. Phase Transition and Lattice Expansion during Hydrogen Loading of Nanometer Sized Palladium Clusters. *J. Alloys Compd.* **2003**, *356*, 644−648.
(73) Iten, R.; Metger, T.; Wilming, H.; del Rio, L.; Renner, R. Discovering Physical Concepts with Neural Networks. *Phys. Rev. Lett.* **2020**, *124*, No. 010508.
(74) Chase, Z. A.; Fulton, J. L.; Camaioni, D. M.; Mei, D.; Balasubramanian, M.; Pham, V. T.; Zhao, C.; Weber, R. S.; Wang, Y.; Lercher, J. A. State of Supported Pd during Catalysis in Water. *J. Phys. Chem. C* **2013**, *117*, 17603−17612.

https://dx.doi.org/10.1021/acs.jpclett.0c03792
J. Phys. Chem. Lett. 2021, 12, 2086−2094